EUROFUSION WPMST1-CP(16) 16574

I Senichenkov et al.

Study of detached H-modes in full tungsten ASDEX Upgrade with N seeding by SOLPS-ITER modeling

Preprint of Paper to be submitted for publication in
Proceedings of 26th IAEA Fusion Energy Conference

This work has been carried out within the framework of the EUROfusion Consortium and has received funding from the Euratom research and training programme 2014-2018 under grant agreement No 633053. The views and opinions expressed herein do not necessarily reflect those of the European Commission.

Study of detached H-modes in full tungsten ASDEX Upgrade with N seeding by SOLPS-ITER modeling

I.Yu.Senichenkov[1], E.G.Kaveeva[1], E.A.Sytova[1], V.A.Rozhansky[1], S.P.Voskoboynikov[1], I.Yu.Veselova[1], A.S.Kukushkin[2,3], D.P.Coster[4], F.Reimold[5], X.Bonnin[6] and the ASDEX-Upgrade Team..
e-mail: I.Senichenkov@spbstu.ru

[1] *Peter the Great St.Petersburg Polytechnic University, 195251, Polytechnicheskaya ul., 29, Saint Petersburg, Russia*
[2] *Kurchatov Institute, Kurchatov sq. 1, 123182 Moscow, Russia,*
[3] *NRNU MEPhI, Kashirskoye sh. 31, 115409 Moscow, Russia*
[4] *Max-Planck Institut für Plasmaphysik, EURATOM Association, D-85748 Garching, Germany*
[5] *Forschungzentrum Jülich GmbH, 52425 Jülich, Germany*
[6] *ITER Organization, CS 90 046, Route de Vinon-sur-Verdon, 13067 St. Paul-lez-Durance, France*

Introduction

Our current understanding of divertor physics indicates that at least partial detachment will be a necessary condition for operation of future fusion power devices such as ITER, DEMO and beyond. In recent years a divertor operation regime with complete detachment was achieved in ASDEX Upgrade with tungsten walls and nitrogen seeding [1-3]. Simultaneously, modeling with the SOLPS5.0 transport code reproduced the main features of these experiments [4], e.g. reduction of the target heat and particle fluxes, strong X-point radiation and moderate pedestal pressure loss. In parallel, additional modeling, aimed at understanding the transition to the detachment regime [5], and using the SOLPS-ITER version of the code [6,7], was performed, however assuming carbon walls, which corresponds to the ASDEX Upgrade experimental condition before changing to a full tungsten wall. This work demonstrated the key role played by the electric field near the X-point [5]. The possible effect of the detached divertor on the radial electric field in the confined region was reported in [8].

In the present paper, the above analysis of the modeling results from the SOLPS-ITER simulations is revisited, but now considering the full tungsten ASDEX Upgrade wall with nitrogen seeding. We consider a range of modeling scenarios by varying the gas puffing and impurity seeding rates. We begin with a reference case with minimal puffing and seeding, which we use to adjust the anomalous transport coefficients so as to match the experimental high-recycling divertor regime with reasonable accuracy. Then, keeping transport coefficients constant we increase the fueling and seeding rates to model a transition to detachment, to study the nitrogen distribution and to compare with previous modeling results obtained earlier for a carbon divertor.

Modeling

The ASDEX Upgrade shot #28903 (described in [4]), was chosen as our reference case, in which the transition to detachment was induced by intensive nitrogen seeding, $\approx 2.5\cdot10^{22}$ electrons/s ($\approx 3.6\cdot10^{21}$ atoms/s), applied at 2.8 s on, while the deuterium fueling rate was kept constant from about 1.3 s on at the level $\approx 2.2\cdot10^{22}$ electrons/s. Instead of modeling the discharge dynamics we consider several steady-state modeling scenarios with different seeding rates in the range from $2\cdot10^{18}$ to $2.0\cdot10^{20}$ atoms/s, thus representing different amounts of nitrogen in the system. The cases with higher seeding rates are not presented due to slow convergence.

In each of these scenarios, in the plasma part of the SOLPS-ITER package (B2.5), drifts and currents are fully turned on for each plasma species (deuterium and nitrogen), while the neutral distribution is modelled by the EIRENE code. The computational domain for the B2.5 and EIRENE codes together with the loci of puffing and pumping are shown in Fig. 1.

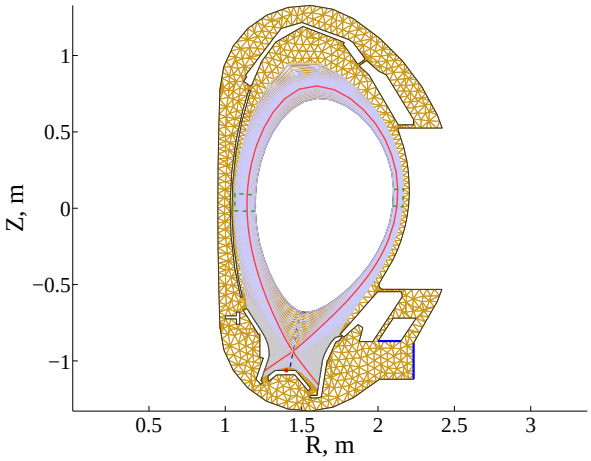

Fig. 1. Computational domain. Blue lines indicate pumps, red bar – locus of puffing, magenta line shows the separatrix.

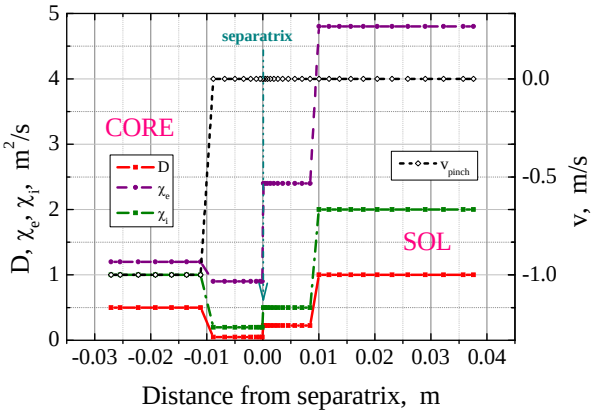

Fig. 2. Anomalous transport coefficients in equatorial midplane

At the core boundary of the computational domain, we prescribe the total heat fluxes in the electron and ion channels (3.2 MW and 1.8 MW correspondingly), zero net deuterium and net nitrogen fluxes (including neutral species modelled by EIRENE), zero net current and an average parallel velocity of -50 km/s (in the co-current direction). Boundary values of D^+ ion and N^{7+} ion densities, both temperatures and the electric potential are fitted to satisfy these boundary conditions. For all other nitrogen ions the condition $\partial n/\partial y = 0$ is used, the condition $\partial u_{\parallel}/\partial y = 0$ is applied for all nitrogen ions.

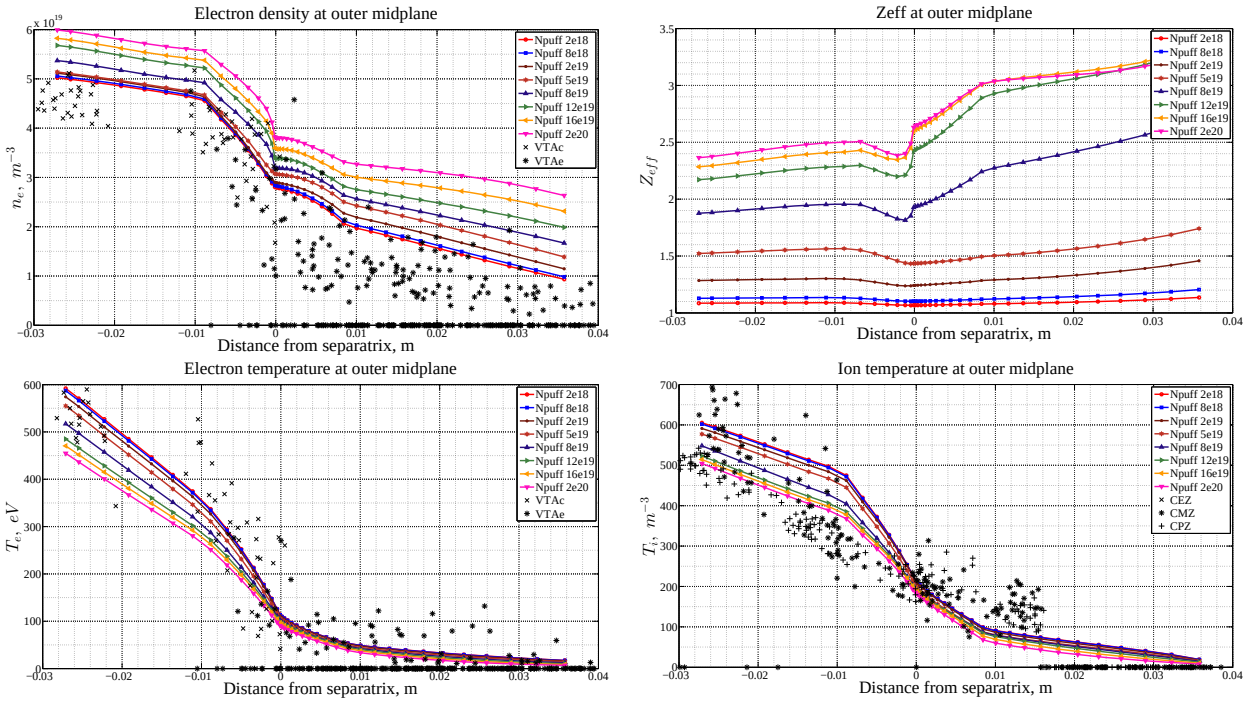

Fig. 3. Calculated profiles at the equatorial midplane. Scattered symbols represent experimental data measured at 2.4 s (before the onset of N-seeding), which correspond to the high-recycling outer target regime.

At the targets, sheath boundary conditions are applied for all main quantities (densities and velocities of charged species, both temperatures and the electric potential).

At the Scrape-off layer (SOL) and Private Flux Region (PFR) boundaries of the B2.5 computational domain the density and temperature decay lengths are prescribed, the condition $\partial u_{\parallel}/\partial y = 0$ is applied for all charged species.

In Fig. 2 are plotted the anomalous transport coefficients along the equatorial midplane, and the modeling results are shown in Figs. 3-6. Note that the transport coefficients in the divertor region (not plotted in Fig. 2) are somewhat bigger, namely $[D, \chi_e, \chi_i] = [8.0, 9.6, 4.0]$ m^2/s, and are radially constant.

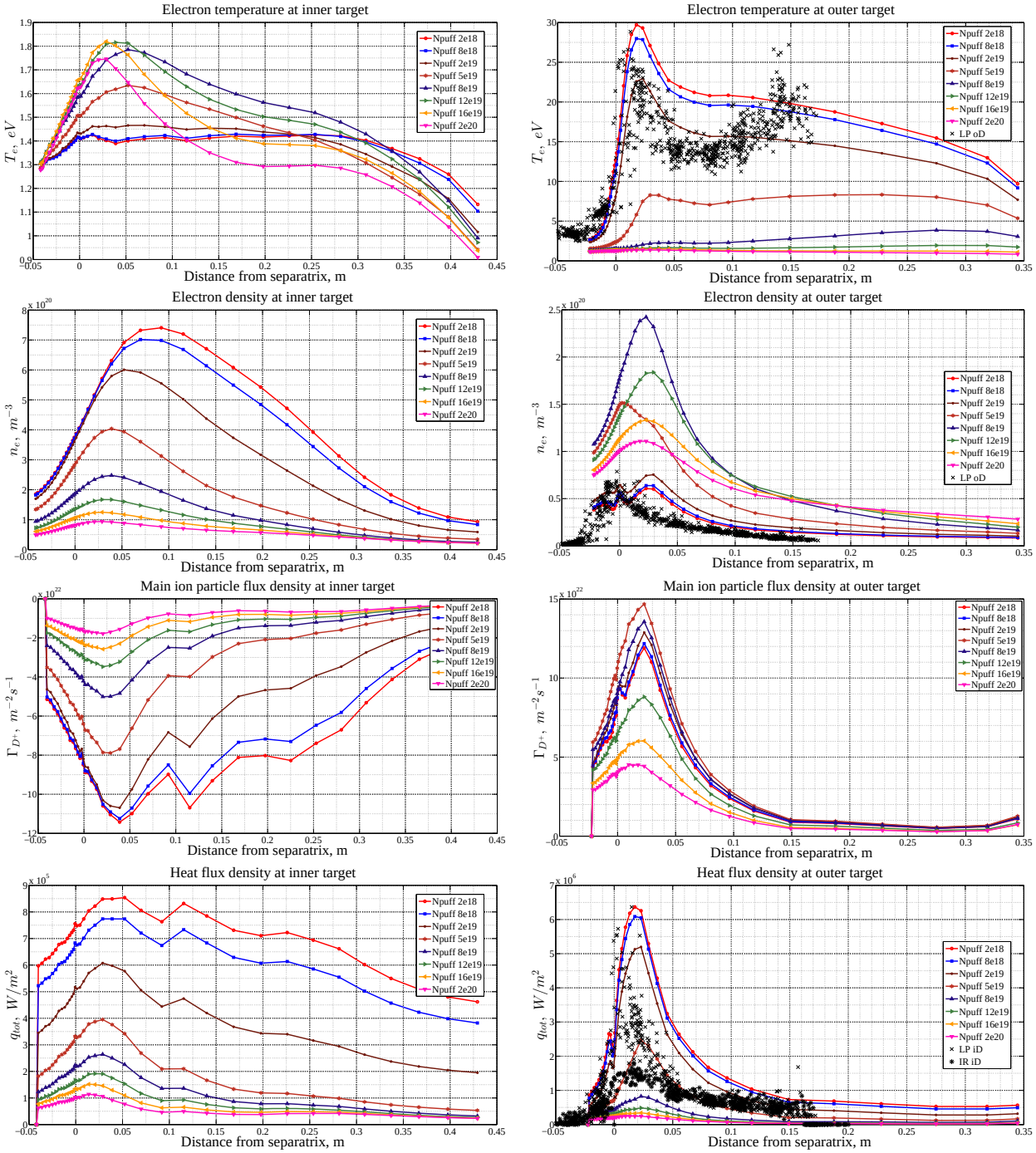

Fig. 4. Calculated profiles at targets. Scattered symbols represent experimental data measured at 2.4 s (before the onset of N-seeding), which correspond to the high-recycling outer target.

One can see the appearance of detachment signs at the seeding rate about $(8 - 12)\cdot 10^{19}$ N atoms per second, which corresponds to about $(1.3 - 1.7)\cdot 10^{19}$ N atoms in the system. These signs are the reduction and flattening of the electron temperature profile and the so-called

rollover in electron density and D^+ ion flux at the outer target, and the reduction (and a sign change) of the net current at both targets. Similar (at least qualitatively) behavior was recently observed in experiments on ASDEX Upgrade [2-4].

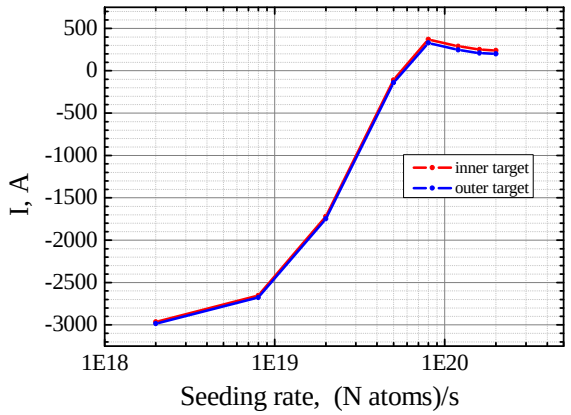

Fig. 5. Calculated net current at targets. Positive sign means that the current is directed from inner to outer target.

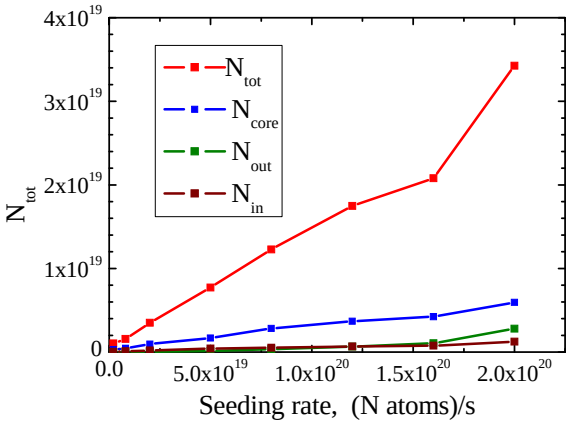

Fig. 6. Total amount of nitrogen nuclei in the confined region and in the whole computatonal domain.

Discussion

To analyze what happens during the transition to detachment in the outer divertor, we start from the nitrogen behavior. One can see from Figs. 3-4 that all three low seeding rate cases satisfactorily agree with experimental data corresponding to the high-recycling regime without any seeding at all. This means that the total amount of nitrogen in the system is so small that nitrogen almost does not affect the plasma profiles in the confined region and at the outer target. The inner target is detached due to the high fueling rate rather than due to seeding.

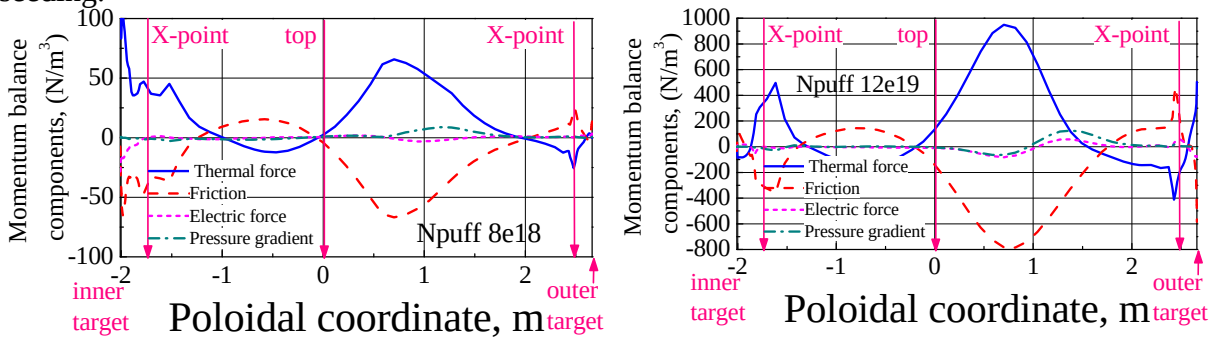

Fig.7 Parallel (along $\vec{B}$) momentum balance for nitrogen (averaged over all nitrogen ions) in the near SOL.

We start our analysis from the nitrogen distribution and transport, which play an important role in the transition to detachment. The parallel velocity of nitrogen is determined from the balance between friction force $R_{\|I} \approx Z^2 n_I n_i m_p \left(V_\| - V_{\|I}\right)\tau_p^{-1}\sqrt{2}$ and thermal force $R_\|^T \approx 1.56 Z^2 n_I \nabla_\| T$ thus giving $V_{\|I} \approx V_\| + 1.56 n_i \tau_p m_p^{-1} \nabla_\| T_i$, as illustrated in Fig. 7, see also [9]. Assuming the parallel velocity of main ions to be positive (i.e. directed towards the target), one may expect that for a hot outer target (like for the seeding rate $8\cdot10^{18}$ at/s) the nitrogen parallel velocity becomes smaller or even negative (i.e. directed upstream). One can see that, as the seeding rate increases, the ion temperature near the outer target decreases, and the nitrogen parallel velocity becomes closer to the parallel velocity of main ions, which is directed towards the target. Thus at the attached outer divertor nitrogen leaks and during transition to the detachment the leakage changes to retention resulting in the nitrogen density

rise and equilibration between the targets, see Fig. 8. The net poloidal nitrogen fluxes in the PFR and SOL, which are directed from the hot outer to the cold inner target for the low seeding rate [9], becomes sign-changing, i.e. vanishes as the nitrogen density increases.

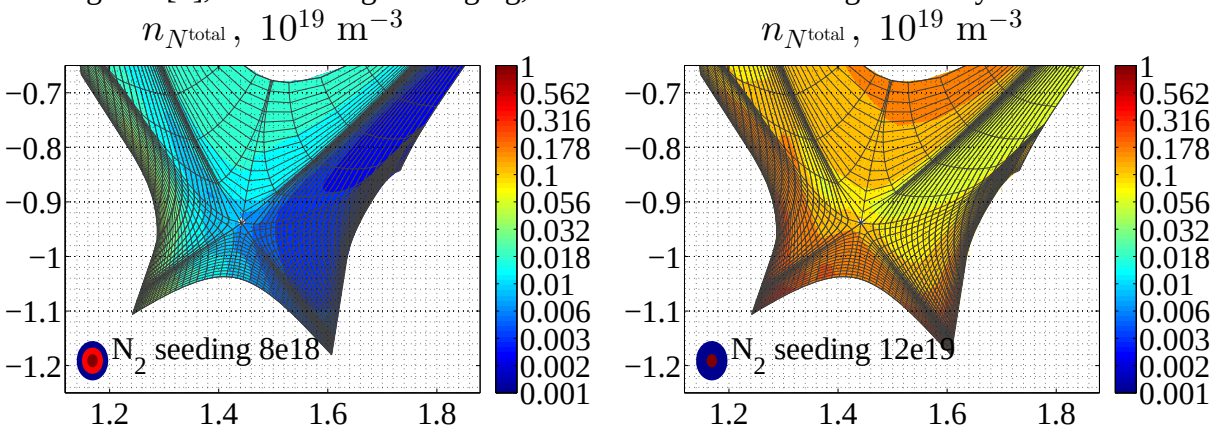

Fig.8. Total nitrogen density (sum over all ionization states) for different seeding rates.

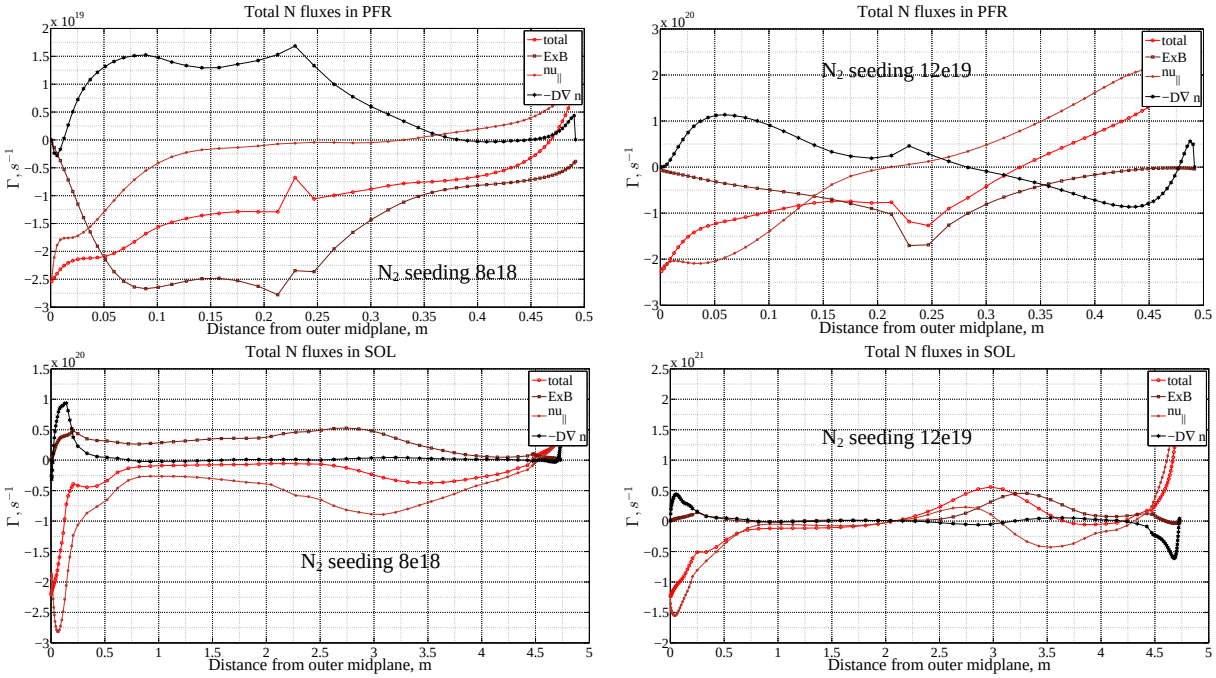

Fig.9. Net poloidal nitrogen flux (sum over all ions, integrated across SOL and PRF) for different seeding rates.

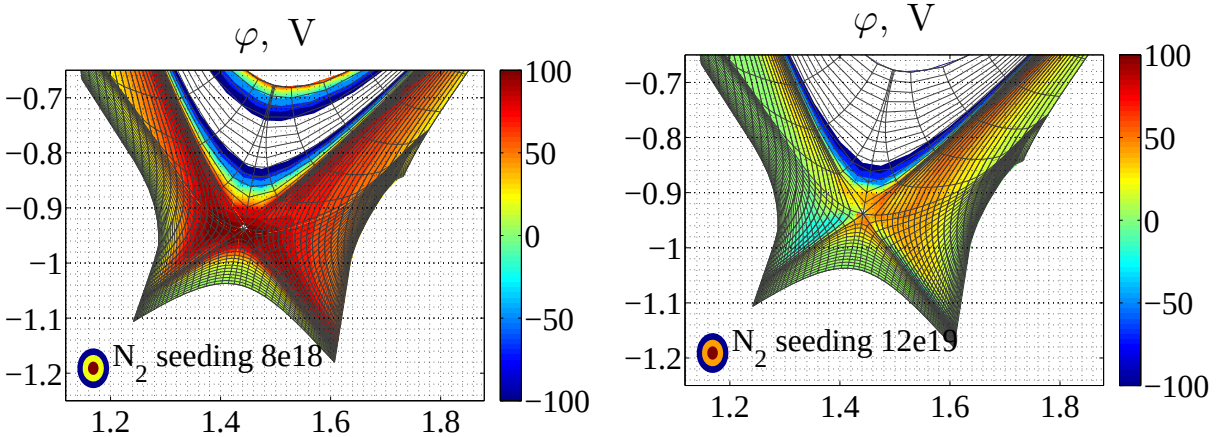

Fig.10. Electric potential.

The outer target cooling and temperature equilibration between targets result in the reduction of thermoelectric current flowing from the hotter plate to the colder one, similarly to experimental observation [3]. This thermoelectric current give the main contribution to the

net poloidal current in the SOL for the low seeding rate scenarios, while for the higher seeding rate ones the thermoelectric current vanishes, and the Pfirsch-Schlüter current that closes the divergent part of ∇B -current becomes the most important. Due to the complicated structure of ∇B -current (the analysis of electric potential, Fig. 10, and current distributions in the divertor region shows that the ∇B -current are closed by the Pfirsch-Schlüter current inside the plasma volume rather than through the targets), it appears that the net current between targets changes its sign and starts to flow from the inner to the outer target.

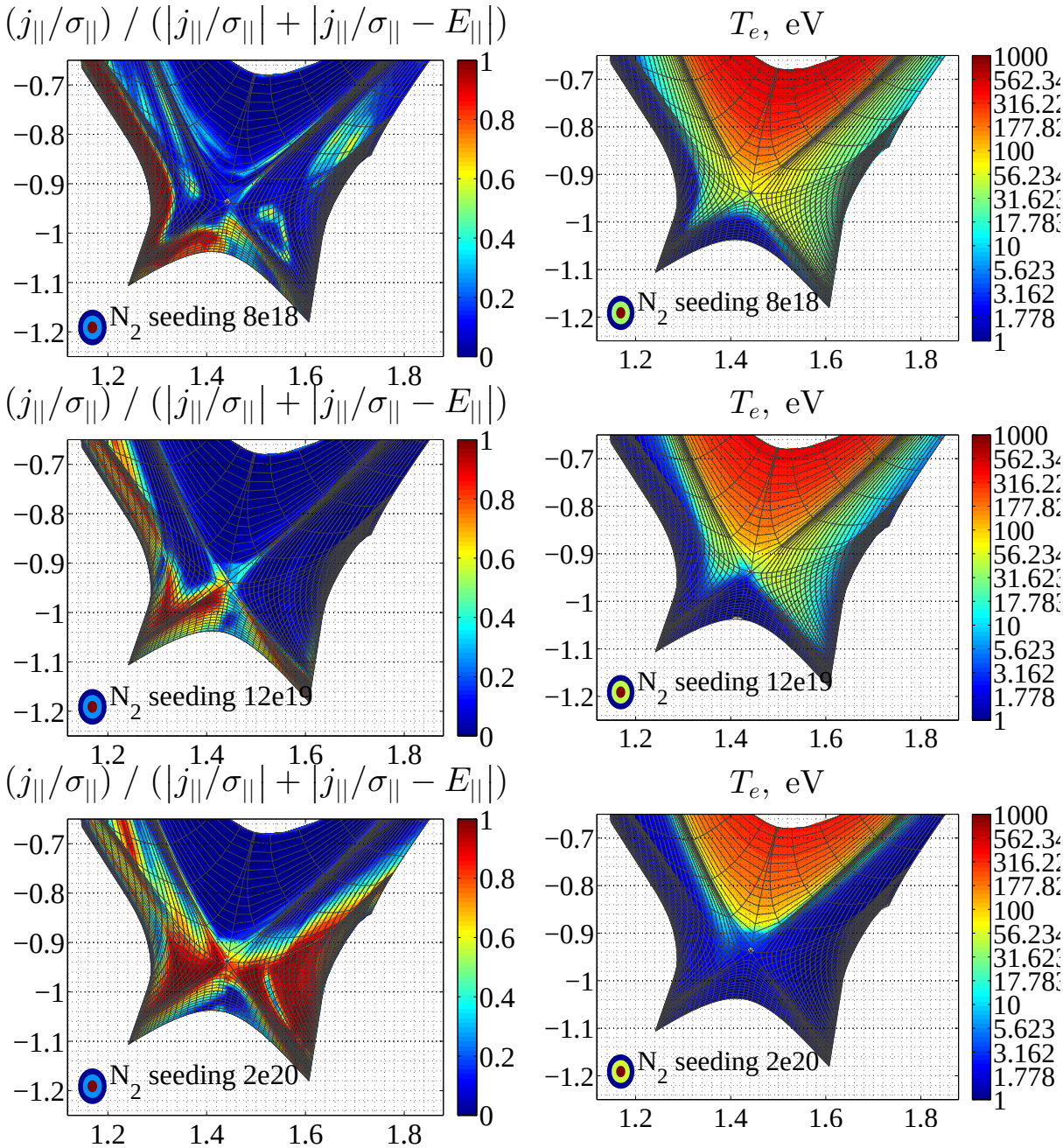

Fig. 11. 2D plots of the T_e and the relative difference between $j_{||}$ and $\sigma_{||}E_{||}$

The requirement to drive the parallel current through the cold plasma of low electric conductivity results in the growth of the poloidal electric field, which reaches the value of 500 V/m while the plasma temperature does not exceed 1-3 eV.

To understand why does this high E-field develop, let's consider Ohm's law $j_{||} = \sigma_{||}\left(E_{||} + \nabla_{||}(n_e T_e)/en_e + 0.71\nabla_{||}T_e/e\right)$. In a high-temperature (and high electric conductivity) plasma the term in parentheses must be relatively small, meaning that the electric field

adjusts to approximately cancel the parallel gradient terms, and the potential is of the order of T_e/e. However, to drive this current through the cold plasma of low electric conductivity near the detached targets, a strong electric field needs to be set up. The potential then exceeds T_e/e significantly, and Ohm's law reduces to $j_{||} = \sigma_{||} E_{||}$. As the seeding rate increases and the outer target detaches, the area of validity of this reduced Ohm's law increases, see Fig. 11.

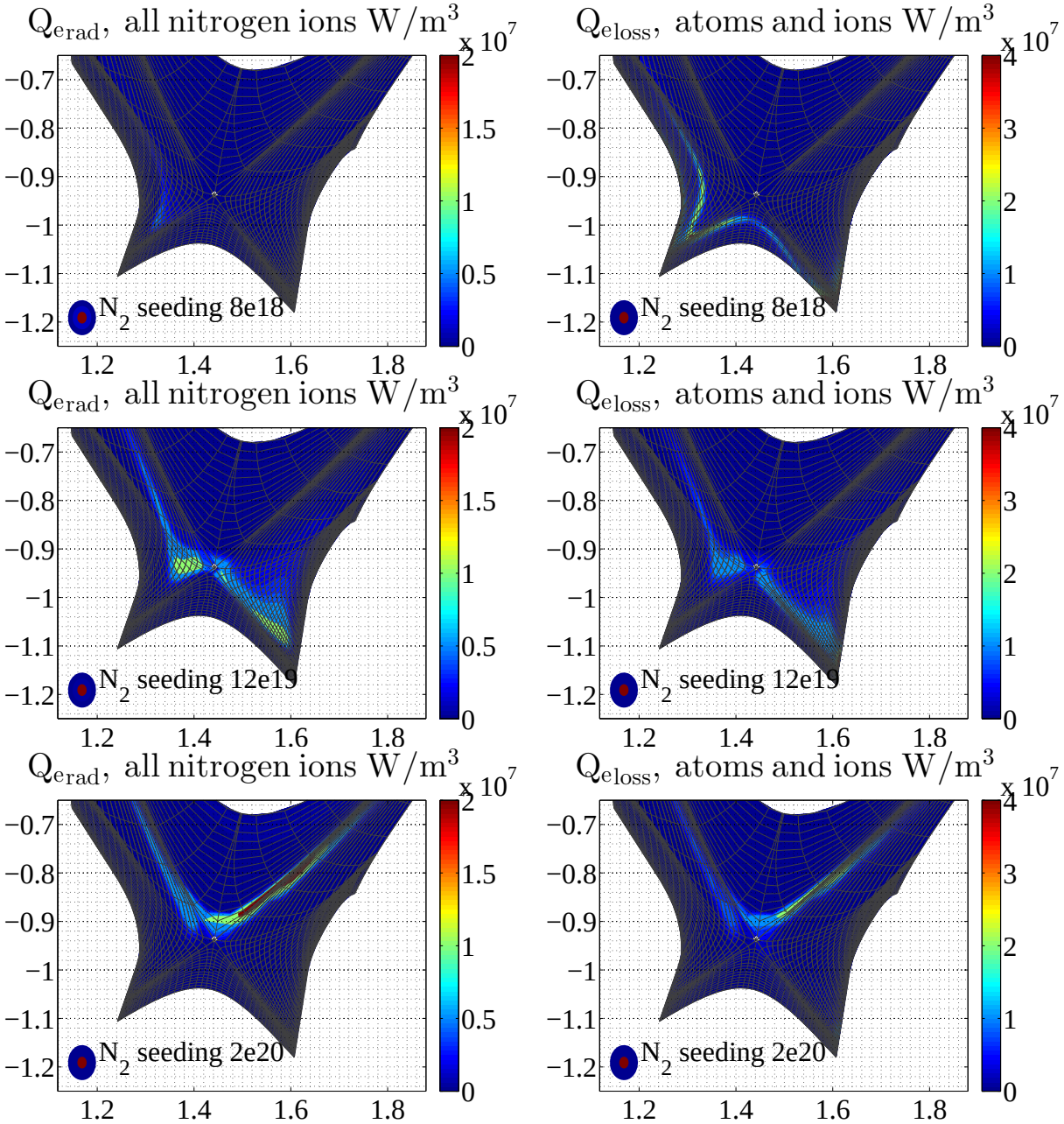

Fig. 12. left: radiated power due to nitrogen ions (excluding nitrogen atoms); right: total electron power losses due to atomic processes.

As the seeding rate increases, the cold region where the temperature is below 5 eV broadens significantly, reaching the X-point from the PFR side and from the HFS of the SOL. Since the boundary of this region is sharp, the ionization of neutrals (and the first two nitrogen ionization states) takes place at this boundary. Due to the same reason the radiation power comes from the same narrow boundary between cold and hot plasma, see Fig. 12. The bigger the seeding rate (and nitrogen content correspondingly), the closer to the X-point does the locus of radiation losses maximum move.

One can see that a seeding rate of even $2 \cdot 10^{20}$ atoms/s is not enough to provide a confined region cooling below 5 eV at least in the X-point vicinity, as it was observed in the

experiment. Note, however, that the experimental seeding rate reaches a value of about $3.6 \cdot 10^{21}$ atoms/s, while corresponding modeling scenarios exhibited poor convergence and are not presented here. The question whether it will be possible to get a stationary solution with such a high amount of nitrogen is left for the near future.

Another problem in modeling results is the too high nitrogen density in the SOL and in the confined region resulting in Z_{eff} exceeding measured values.

Conclusions

A series of steady state modeling scenarios corresponding to the ASDEX Upgrade N-seeded plasma was performed with the SOLPS-ITER code. The transport equations are taken in the SOLPS5.2 form (see [10]), and all drift and current terms are turned on. By varying the nitrogen seeding rate from one scenario to another the total nitrogen amount inside the vacuum vessel is controlled, thus the transition to detachment observed in the experiment after turning the seeding on is modelled.

The experimental conditions corresponding to the high-recycling regime at the outer target with zero seeding rate are reproduced in low seeding rate modeling scenarios almost independently of the seeding rate value while it remains much smaller than the experimental value $3.6 \cdot 10^{21}$ atoms/s. It is demonstrated that the $E \times B$ drift gives a significant contribution to the nitrogen fluxes in the SOL and in the PFR.

During the transition to the detachment at the outer target with increasing seeding rate/nitrogen content, the following experimentally observed features are reproduced: i) reduction and even sign inversion of the net current through the divertor plates; ii) roll-over in electron density and main ion particle flux at the outer target; iii) appearance of the radiating spot near the X-point vicinity, iv) appearance of the cold and dense plasma near in the target vicinity, which broadens towards the X-point with increasing seeding rate. Inside this cold and dense region with low Spitzer conductivity a strong E-field develops in order to drive Pfirsch-Schlüter currents there.

A seeding rate of $2.0 \cdot 10^{20}$ atoms/s is not enough to provide the cooling of the confined region even in the X-point vicinity and the ability for neutrals to penetrate there. No significant radiative losses from the confined region and no confinement reduction are observed in the corresponding modeling scenario despite the fact that the nitrogen content (and Z_{eff}) exceeds the experimental value.

Results from runs of another scenarios with increased seeding rate (up to the experimental value), which are time consuming and converge slowly, are required for further understanding and are expected in the near future.

Acknowledgements

The work is supported by Russian Ministry of Education and Science, Agreement No. 14.619.21.0001. Computations are performed in the SPbPU Supercomputer Center. The views and opinions expressed herein do not necessarily reflect those of the ITER Organization.

References

[1] S. Potzel *et al* Nucl. Fusion **54** (2014) 013001
[2] F. Reimold *et al* Nucl. Fusion **55** (2015) 033004
[3] A. Kallenbach *et al* Nucl. Fusion **55** (2015) 053026
[4] F. Reimold *et al* Journal of Nuclear Materials 463 (2015) 128–134
[5] I. Senichenkov *et al*, EPS conference 2015, ECA Vol. **39E** P5.191
[6] S. Wiesen *et al* Journal of Nuclear Materials 463 (2015) 480–484
[7] X. Bonnin *et al* Plasma and Fusion Research 11 (2016) 1403102
[8] E. Sytova *et al*, H-mode workshop, Garching, Germany 2015
[9] E. Sytova *et al,* EPS conference 2016, ECA Vol. **40E** P1.054
[10] V. Rozhansky et al. Nucl. Fusion **49** (2009) 0250007 (11pp)